Polymer Chemistry

pH- and Chaotropic Anion-Induced Conformational Changes of Tertiary Amine-Containing Binary Heterografted Star Molecular Bottlebrushes in Aqueous Solution

Journal:	*Polymer Chemistry*
Manuscript ID	PY-ART-10-2020-001466.R1
Article Type:	Paper
Date Submitted by the Author:	14-Nov-2020
Complete List of Authors:	Kent, Ethan; The University of Tennessee, Department of Chemistry Lewoczko, Evan; University of Tennessee, Chemistry Zhao, Bin; The University of Tennessee, Department of Chemistry

pH- and Chaotropic Anion-Induced Conformational Changes of Tertiary Amine-Containing Binary Heterografted Star Molecular Bottlebrushes in Aqueous Solution

*Ethan W. Kent, Evan M. Lewoczko, and Bin Zhao**

Department of Chemistry, University of Tennessee, Knoxville, Tennessee 37996, United States

* Corresponding author. Email: bzhao@utk.edu

Abstract. This article reports on the conformational behavior of binary heterografted three-arm star molecular bottlebrushes composed of poly(ethylene oxide) (PEO) and either poly(2-(*N,N*-dimethylamino)ethyl methacrylate) (PDMAEMA, the brushes denoted as SMB-1) or poly(2-(*N,N*-diethylamino)ethyl methacrylate) (PDEAEMA, the brushes denoted as SMB-2) side chains in aqueous solutions in response to pH changes and addition of salts containing chaotropic anions (CAs). PEO was introduced into the brushes as a stabilizer when the tertiary amine-containing side chains collapsed. While a small size decrease of SMB-1 was observed with increasing pH from acidic to basic, SMB-2 exhibited a large and abrupt size transition caused by the pH-induced solubility change of PDEAEMA. Atomic force microscopy imaging revealed a star-to-globule shape transition of SMB-2 upon increasing pH across the pK_a; in contrast, SMB-1 stayed in the starlike state at both low and high pH values. Intriguingly, both SMB-1 and -2 displayed star-to-globule shape transitions in acidic solutions upon addition of salts containing sufficiently strong CAs such as ClO_4^-, with SMB-2 showing a greater sensitivity to moderate CAs than SMB-1. Moreover, superchaotropic anions (e.g., $Fe(CN)_6^{3-}$ and $S_2O_8^{2-}$) were significantly more efficient in inducing shape changing than common CAs. The CA-induced shape transitions resulted from the

ion pairing of CAs and protonated tertiary amine groups and the high propensity of CAs to associate with hydrophobic moieties in the brushes, which decreased the solubility of the tertiary amine-containing side chains and caused the brushes to collapse. The findings reported here may enable potential applications of molecular bottlebrushes in, e.g., encapsulation and release of ionic substances.

Introduction

Molecular bottlebrushes (MBBs) are a class of architecturally complex macromolecules featured by relatively short polymeric side chains densely tethered on a long backbone polymer via a covalent bond.[1-5] The dense grafting of side chains is the origin of many unique characteristics and behavior exhibited by MBBs,[1-9] including large and tunable persistence length,[6] no or very low chain entanglement,[7] high density of functional groups,[8] unusual crystal habit,[9] etc. The molecular geometry and dimensions of MBBs are determined by the lengths of backbone and side chain polymers, grafting density of side chains, brush architecture, and environmental conditions.[3] In good solvents, the excluded volume interactions of the polymeric side chains cause the MBBs to adopt stretched cylindrical conformations. When the surrounding conditions change, MBBs can display pronounced conformational changes (or shape transitions), e.g., from wormlike to globular.[10] The large sizes and anisotropic shapes of MBBs allow for easy visualization and convenient examination of their conformational behavior at the single-molecule level by atomic force microscopy (AFM) and transmission electron microscopy (TEM).[1-5]

The intriguing conformational changes of MBBs have been demonstrated at interfaces and in solution.[10-30] Sheiko et al. reported that MBBs with homografted poly(*n*-butyl acrylate) (P*n*BA) side chains underwent reversible rod-to-sphere shape transitions at the air-water interface in a Langmuir-Blodgett trough upon lateral compression and expansion.[10] Using environmentally controlled AFM, Möller et al. observed reversible worm-to-globule shape transitions of P*n*BA MBBs in situ on solid substrates in real time upon introduction of different solvent vapors into the environmental chamber.[12,13] When stimuli-responsive polymers are employed as side chains,[4,14-25] the shape transitions of MBBs can be induced in solution by external stimuli. Schmidt et al. synthesized the first thermoresponsive MBBs via a "grafting from" approach using atom transfer

radical polymerization (ATRP) to grow poly(*N*-isopropylacrylamide) (PNIPAm) side chains from pendant initiating sites of a macroinitiator and found that the obtained brush polymer exhibited a worm-to-globule shape transition upon heating.[14] However, the collapsed globular PNIPAm MBBs were unstable at temperatures above the lower critical solution temperature (LCST); the brushes aggregated and eventually precipitated out from the solution. Polyelectrolyte MBBs have been shown to exhibit rich conformational behavior in aqueous solution in response to the addition of surfactants, oppositely charged linear polyelectrolytes, and multivalent ions.[19,26-30] Müller et al. reported that the complexation of cationic MBBs with sodium dodecyl sulfate (SDS) in dilute conditions led to a wormlike-to-globular shape transition.[27] Addition of β-cyclodextrin, which can form an inclusion complex with SDS, switched the globular brushes back to wormlike; the brushes collapsed again when a more competitive inclusion agent was used. At a slightly higher concentration (e.g., 1 mg/mL), the brushes precipitated out immediately after the addition of SDS. Intriguing helical conformations of polyelectrolyte MBBs in highly dilute aqueous solutions were also observed by AFM and TEM after the addition of multivalent ions or surfactants.[28-30]

Stimuli-responsive shape-changing MBBs have potential in many applications, such as encapsulation and release of (drug) substances, regulation of molecular interactions and assembly, viscosity control, etc. However, to effectively utilize shape-changing MBBs in any possible applications, one must achieve the stabilization of collapsed globular brushes in solution. By introducing a second polymer into the side chains of MBBs, either as a distinct set of side chains in heterografted brushes[31,32] or as the outer block of diblock copolymer side chains in homografted MBBs,[33] we showed that the resultant bicomponent MBBs underwent shape transitions between wormlike and collapsed yet stable globular conformations in aqueous solutions, where the second polymer in the side chains served as a stabilizer. When both side chain polymers in binary

heterografted MBBs were stimuli-responsive, two distinct stable globular states were obtained under different conditions.[34] Moreover, we demonstrated that unimolecular shape transitions were possible in moderately concentrated aqueous solutions when the stabilizing side chains were much longer than the responsive side chains.[35] Note that all of our brush polymers were synthesized by a grafting-to method using the highly efficient copper(I)-catalyzed alkyne-azide cycloaddition (CuAAC) reaction, which is a modular approach allowing for facile incorporation of different side chain polymers and tuning of their molar ratios.[9,31-42]

In the present work, we synthesized binary heterografted star MBBs composed of poly(ethylene oxide) (PEO) and a tertiary amine-containing polymer, either poly(2-(*N*,*N*-dimethylamino)ethyl methacrylate) (PDMAEMA, the corresponding MBBs denoted as SMB-1) or poly(2-(*N*,*N*-diethylamino)ethyl methacrylate) (PDEAEMA, the corresponding MBBs denoted as SMB-2), as side chains using the CuAAC reaction (Scheme 1). While SMB-1 showed a small size reduction and no shape change in aqueous solution with increasing pH from below to above the pK_a, SMB-2 exhibited a pH-induced starlike-to-stable globular shape transition with the PEO side chains acting as a stabilizer. Moreover, we report here a new shape changing mechanism; both brush polymers underwent drastic shape transitions in acidic aqueous solutions in response to the addition of salts containing sufficiently strong chaotropic anions (CAs) such as ClO_4^- (Scheme 1). CAs usually have a large size and a relatively low charge density; they are water-structure breakers, meaning that the water molecules surrounding them are less hydrogen bonded and have a higher entropy compared with bulk water.[43-46] Chaotropic cations and anions tend to form tight ion pairs in water.[44-48] These ions, particularly (super)chaotropic anions, exhibit a high propensity to associate with hydrophobic surfaces, interfaces, macrocyclic binding sites, and organic polymers in aqueous solution, which is termed as chaotropic effect and has emerged as a generic driving

force for supramolecular self-assembly.[46] The underlying mechanisms of both chaotropic ion pairing and chaotropic effect lie in the release of water molecules surrounding (super)chaotropic ions into bulk solution to form stronger water-water interactions.

Scheme 1. Synthesis of Tertiary Amine-Containing Binary Heterografted Star Molecular Bottlebrushes, SMB-1 and SMB-2, via Copper(I)-Catalyzed Azide-Alkyne Cycloaddition (CuAAC) Reaction and Shape Transitions Induced pH Changes and Chaotropic Anions

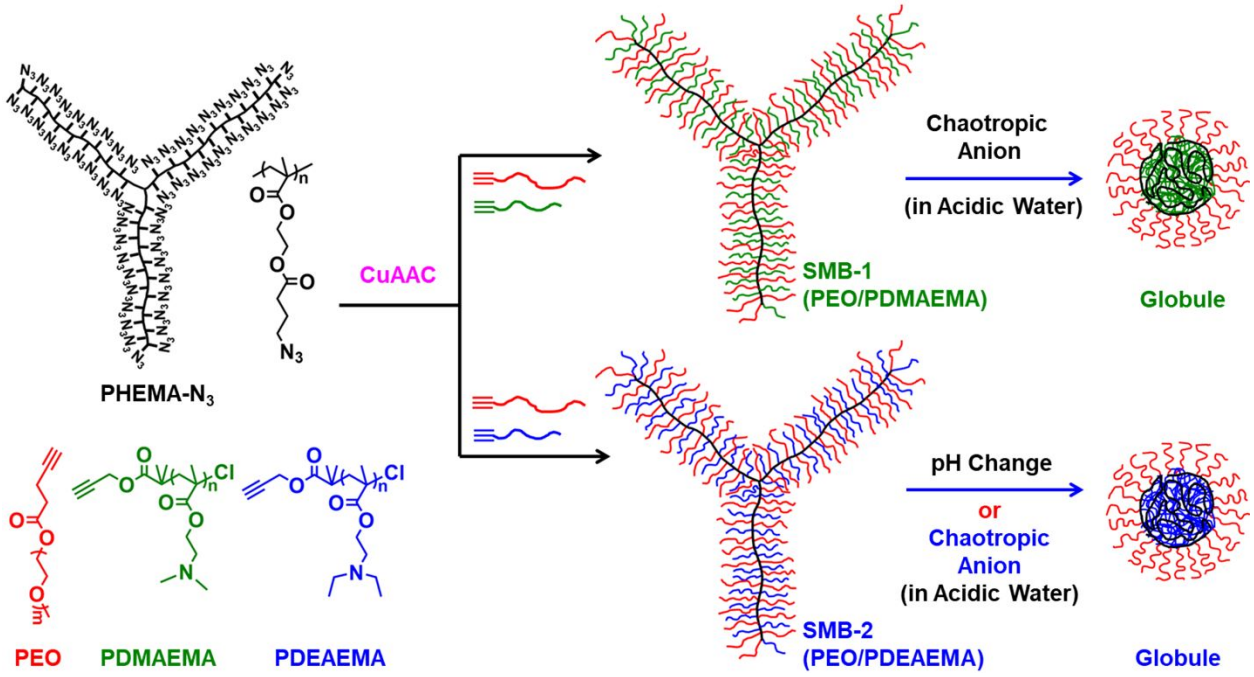

Results and Discussion

Synthesis of Binary Heterografted Star MBBs with PEO and Tertiary Amine-Containing Polymethacrylate Side Chains: SMB-1 and SMB-2. Three-arm star MBBs were prepared by simultaneously grafting two alkyne-end-functionalized polymers, PEO and either PDMAEMA (for SMB-1) or PDEAEMA (for SMB-2), onto the azide-functionalized star backbone polymer, PHEMA-N_3, via the highly efficient CuAAC click reaction (Scheme 1). The detailed synthesis of star backbone PHEMA-N_3, with a DP of 434 per arm, was reported previously.[34] Briefly, an ATRP

of 2-(trimethylsilyloxy)ethyl methacrylate was conducted from a trifunctional initiator, followed by a series of post-polymerization reactions to install azide functional groups on the backbone; these include the removal of trimethylsilyl protecting groups, esterification of the deprotected hydroxyl groups with 4-bromobutyryl chloride, and finally substitution of the pendant bromide groups with azide via reaction with sodium azide. ^{1}H NMR analysis showed a degree of azide functionalization of 88.3%. Alkyne-end-functionalized PEO was made by a carbodiimide-mediated reaction between poly(ethylene oxide) monomethyl ether with a molecular weight of 5000 Da and 4-pentynoic acid.[31] ^{1}H NMR spectroscopy analysis of the purified PEO indicated quantitative end group functionalization (Figure S1A), and size exclusion chromatography (SEC) analysis revealed a narrow monomodal peak with a $M_{n,SEC}$ of 8.3 kDa and a dispersity ($Đ$) of 1.04 (Figure S1B) (Table 1).

Table 1. Characterization Data for Star Backbone Polymer PHEMA-N_3, Alkyne End-Functionalized Side Chain Polymers (PEO, PDMAEMA, and PDEAEMA), and Star Molecular Bottlebrushes (SMB-1 and -2).

Polymer Sample	DP or Grafting Density (σ)	Molecular Weight and $Đ$
PHEMA-N_3	DP = 434 per arm [a]	$M_{n,SEC} = 2.25 \times 10^5$ Da, $Đ = 1.16$ [d]
PEO	DP = 114 [b]	$M_{n,SEC} = 8.3 \times 10^3$ Da, $Đ = 1.04$ [d]
PDMAEMA	DP = 45 [a]	$M_{n,SEC} = 1.12 \times 10^4$ Da, $Đ = 1.17$ [d]
PDEAEMA	DP = 42 [a]	$M_{n,SEC} = 1.07 \times 10^4$ Da, $Đ = 1.18$ [d]
SMB-1 (PEO/PDMAEMA)	σ = 85.3% [c]	$M_{w,exp} = 9.71 \times 10^6$ Da [e] $M_{w,cal} = 7.86 \times 10^6$ Da [f]
SMB-2 (PEO/PDEAEMA)	σ = 84.8% [c]	$M_{w,exp} = 9.08 \times 10^6$ Da [e] $M_{w,cal} = 8.25 \times 10^6$ Da [f]

[a] Degree of polymerization (DP) was calculated from the monomer conversion, determined by ^{1}H NMR analysis, and the monomer-to-initiator molar ratio. [b] The DP of PEO was calculated from the molecular weight (5000 g/mol). [c] The value of grafting density (σ) was estimated using the ratio of SEC peak areas of the brushes and the unreacted side chain polymers in the final reaction mixture, the feed ratios of the backbone polymer to the side chain polymers, and the side chain composition of the final brushes from ^{1}H NMR analysis. [d] $M_{n,SEC}$ and $Đ$ were determined by SEC relative to polystyrene standards. [e] The experimental absolute molecular weight ($M_{w,exp}$) was determined by SEC using a SEC-MALS system. [f] The calculated absolute molecular weight ($M_{w,cal}$) was obtained by considering the weight-average molecular weight of PHEMA-N_3 and the side chain polymers, calculated from the DP and the dispersity ($M_n \times Đ$), and the σ.

Alkyne end-functionalized tertiary amine-containing side chain polymers, PDMAEMA and PDEAEMA, were synthesized by ATRP of respective methacrylate monomers in anisole at 50 °C using propargyl 2-bromoisobutyrate as the initiator and CuCl/1,1,4,7,10,10-hexamethyltriethylenetetramine as the catalyst/ligand. SEC analysis showed a narrow unimodal peak for both polymers, indicating that the polymerizations were controlled; for PDMAEMA, $M_{n,SEC}$ = 11.2 kDa and $Đ$ = 1.17 (Figure S2A), and for PDEAEMA, $M_{n,SEC}$ = 10.7 kDa and $Đ$ = 1.18 (Figure S3A), relative to polystyrene standards. The degrees of polymerization (DPs) of PDMAEMA and PDEAEMA were 45 and 42, respectively, calculated from the monomer conversions and the monomer-to-initiator feed ratios. The detailed synthesis and characterization of PDMAEMA and PDEAEMA can be found in the Supporting Information (Figures S2 and S3), and the characterization data are summarized in Table 1 along with the data for PHEMA-N_3.

The click reactions for the synthesis of star MBBs were carried out in THF at room temperature under a nitrogen atmosphere using CuCl and *N*,*N*,*N*′,*N*″,*N*″-pentamethyldiethylenetriamine as the catalyst and ligand, respectively. For SMB-1, the feed molar ratios of PHEMA-N_3 repeat units to PEO and PDMAEMA side chains were 1 : 0.55 : 0.54. For SMB-2, the feed ratios of PHEMA-N_3 repeat units to PEO and PDEAEMA were 1 : 0.58 : 0.64. After the reactions proceeded for 22-23 h, propargyl benzyl ether was injected into the mixtures to attempt to cap the possible unreacted azide groups on the backbone. The reaction mixtures were passed through a basic alumina/silica gel column to remove the copper catalyst and the brush polymers were purified by multiple rounds of centrifugal filtration at 5000 rpm using 50 kDa MWCO centrifugal filters with a mixture of water and ethanol (50/50, v/v) as the solvent. The removal of unreacted side chain polymers was confirmed for both brush polymers by SEC analysis (Figure S4).

^{1}H NMR spectroscopy analysis revealed that SMB-1 was composed of 54.3 mol% PEO and

45.7 mol% PDMAEMA side chains, calculated by using the integrals of the peaks at 4.25 – 3.94 ppm (-COOCH_2- of PDMAEMA) and 3.37 ppm (-OCH_3 of PEO) and their DPs (Figure S5A). The molar ratio of two side chain polymers in the brushes was close to that in the feed, although there were slightly more PEO side chains. By using the SEC peak areas of the brushes (78.0 %) and the remaining side chain polymers (22.0 %) from the final reaction mixture (Figure S4A), the feed molar ratios, and the composition of the side chain polymers in the purified brushes from the ^{1}H NMR analysis, the grafting density (σ) of SMB-1 was calculated to be 85.3 %. A detailed description of the calculation is included in the Supporting Information. The experimental absolute molecular weight ($M_{w,exp}$) of SMB-1 was found to be 9.71×10^6 Da, determined by SEC analysis using a SEC-MALS system equipped with a two-angle light scattering detector in series with an RI detector (Figure S5B). Considering the weight-average molecular weight of PHEMA-N_3 and the side chain polymers, calculated from the DP and the dispersity ($M_n \times Đ$), and the grafting density, the calculated $M_{w,cal}$ was 7.86×10^6 Da. The discrepancy between the $M_{w,exp}$ and the $M_{w,cal}$ might come from the loss of lower molecular weight brush molecules during the seven rounds of centrifugal filtration to remove unreacted side chain polymers; we found from SEC analysis the presence of brush molecules in the filtrate in the synthesis of other binary heterografted brush polymers despite the use of 50 kDa MWCO centrifuge filter units.

SMB-2, composed of PEO and PDEAEMA side chains, was synthesized and purified in a similar manner. ^{1}H NMR analysis showed that SMB-2 contained 53.9 mol% PEO and 46.1 mol% PDEAEMA side chains (Figure S6A). From the SEC peak areas for the brushes (68.3 %) and the unreacted side chain polymers (31.7 %) (Figure S4B), the overall grafting density of SMB-2 was calculated to be 84.8%. The experimental absolute $M_{w,exp}$ of SMB-2 from SEC analysis using a SEC-MALS system was 9.08×10^6 Da (Figure S6B), which was closer to but still higher than the

$M_{w,cal}$ of 8.25 × 10^6 Da, likely due to the same reason as for the observation of SMB-1. The characterization data for SMB-1 and SMB-2 are summarized in Table 1 along with the calculated absolute weight-average molecular weights.

The success in the synthesis of star MBBs by the CuAAC reactions was further confirmed by AFM imaging of the brush molecules spin cast onto freshly cleaved mica from their THF solutions (Figures 1, S7, and S8). For both brushes, a vast majority of the brushes were star-shaped with three arms, although some molecules had either a missing arm or a rather short arm, which might be caused by the mechanical shear force during the preparation of AFM samples. Using the ImageJ software, the average arm length was 92.9 ± 27.3 nm for SMB-1 and 94.1 ± 30.3 nm for SMB-2 (300 arms measured for each), with a typical height of ~ 1.5 nm for both brush polymers. Since each arm of the backbone has a calculated DP of 434, the measured average length from the AFM images represents a degree of stretching of 84.2 % for SMB-1 and 85.3 % for SMB-2.

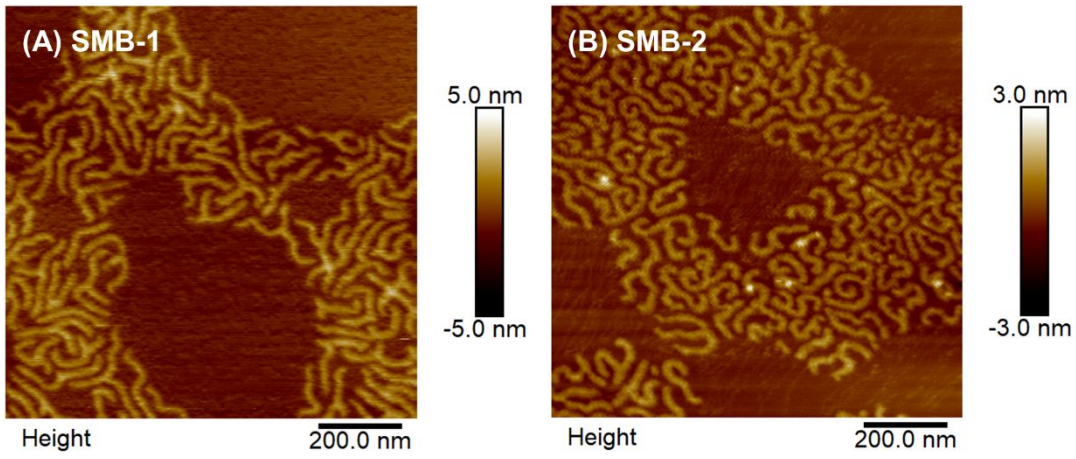

Figure 1. AFM height images of SMB-1 (A) and SMB-2 (B) spin cast onto freshly cleaved bare mica from 0.01 mg/g solutions of the corresponding brush polymers in THF.

Behavior of SMB-1 and -2 in Response to pH Changes. We first investigated the behavior of SMB-1 and -2 in aqueous solutions in response to pH variations. PDMAEMA and PDEAEMA both exhibit a pK_a value of ~ 7.4 in water;[49] however, they respond differently to pH changes.[49-51] PDMAEMA is soluble in both acidic and basic aqueous solutions, whereas PDEAEMA is a pH-responsive water-soluble polymer, displaying a pronounced soluble-to-insoluble transition in water when the solution pH is increased from below to above its pK_a. Figure 2A shows the apparent hydrodynamic diameter (D_h) as a function of pH for a 0.2 mg/g solution of SMB-1 in a 10 mM phosphate buffer at 25 °C from a DLS study. The solution pH was gradually changed using 0.1 M HCl and 0.1 M NaOH at room temperature under the stirring conditions prior to DLS measurements. From pH = 4.00 to 7.50, SMB-1 exhibited little change in the D_h, with a D_h value of 85.2 nm at the pH of 4.00 and 82.4 nm at the pH of 7.50. This was followed by a sharp, albeit small, reduction in size to 75.2 nm at pH = 8.00, above which the D_h leveled off and reached 74.6 nm at pH = 9.50. Throughout the pH range studied, a single, narrow size distribution was observed, indicating that the SMB-1 brush molecules did not undergo aggregation in the solution; Figure 2B shows the hydrodynamic size distributions at pH = 4.00 and 9.50. The observed sharp, although small, size change occurred at the pH values around the reported pK_a of PDMAEMA (~7.4). At pH < pK_a, the majority of tertiary amine groups were protonated, resulting in strong electrostatic repulsive interactions between the PDMAEMA side chains and further stretching of the brush molecules in the solution. When the pH was raised to above the pK_a, most of the PDMAEMA repeat units were deprotonated; consequently, the electrostatic repulsion between the side chains diminished, causing the brush molecules to contract slightly in water.

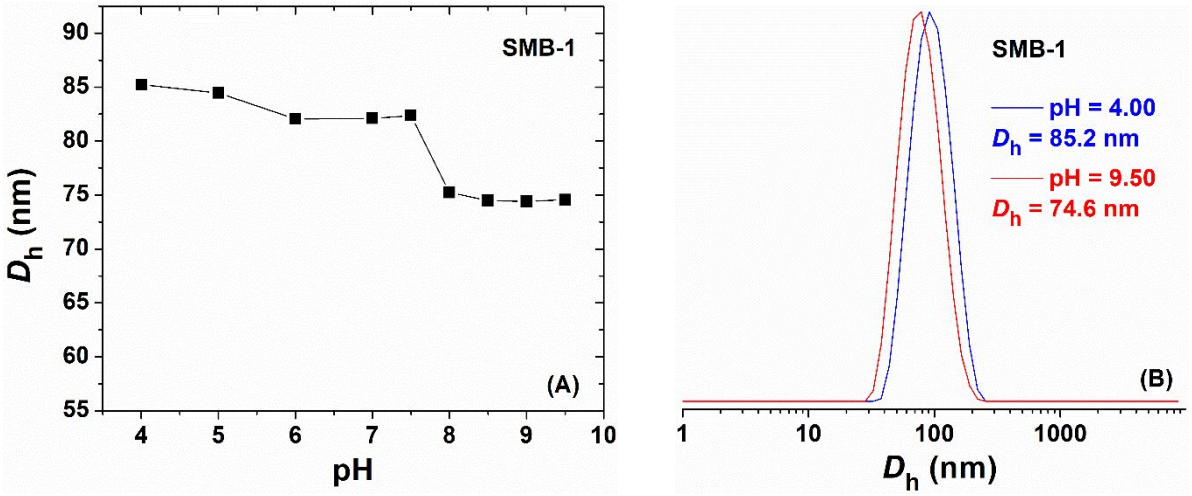

Figure 2. (A) Apparent hydrodynamic diameter (D_h) of SMB-1 at a concentration of 0.2 mg/g in a 10 mM phosphate buffer solution at 25 °C as a function of pH from a dynamic light scattering study. (B) Hydrodynamic size distributions of SMB-1 at pH = 4.00 and pH = 9.50.

As shown in Figure 2A, the pH-induced change in the D_h of SMB-1 was only 10.6 nm, suggesting shrinking of the brush molecules at higher pH values, instead of full collapse into a compact globular state. This was confirmed by AFM imaging of SMB-1 brush molecules spin cast onto glass substrates from 0.05 mg/g aqueous solutions with pH values of 4.00 and 9.50. At pH = 4.00 (Figures 3A and S9), the brushes were in a starlike state, as expected, with an average arm length of 99.7 ± 24.7 nm (75 arms measured). At the pH of 9.50 (Figures 3B and S10), the brush molecules were also in a starlike conformation and the average arm length was 98.9 ± 25.7 nm (75 measured). These observations are consistent with the literature report that PDMAEMA is a water-soluble polymer in the entire pH range. The somewhat similar average arm lengths of SMB-1 at the two different pH values might be partly due to the surface stretching effect during the preparation of AFM samples by spin casting.

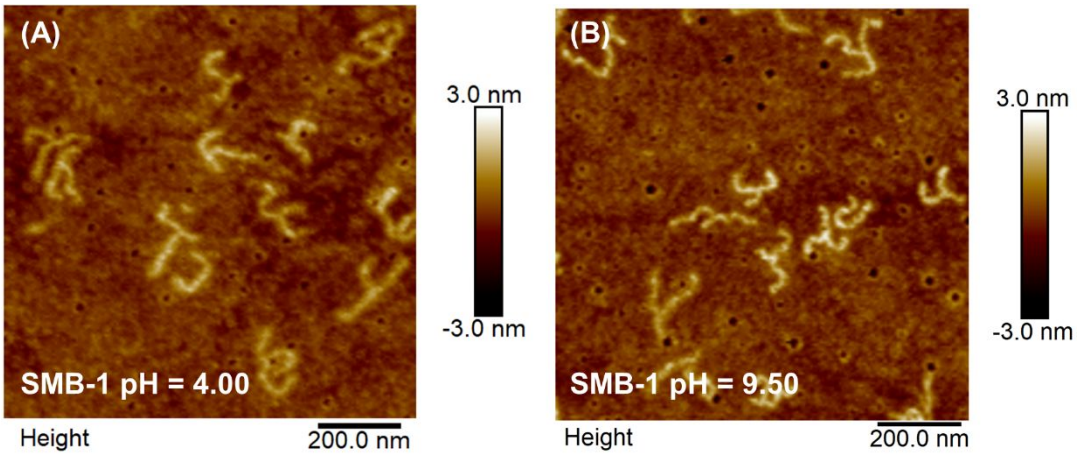

Figure 3. AFM height images of SMB-1 spin cast onto a glass disk from 0.05 mg/g aqueous solutions with (A) a pH of 4.00 and (B) a pH of 9.50.

Figure 4A shows the plot of D_h versus pH for SMB-2 at a concentration of 0.2 mg/g in a 10 mM phosphate buffer at 25 °C. Upon increasing pH from 3.95 to 6.91, the D_h decreased slightly from 88.2 to 82.5 nm, followed by a sharp reduction to 63.6 nm at pH = 7.51. Above the pH of 7.51, there was only a very small change in size and the D_h reached 59.6 nm at pH = 9.50. Overall, the change in the D_h from pH = 3.95 to 9.50 was 28.6 nm, much larger than that of SMB-1 (10.6 nm). It should be noted here that at all studied pH values the hydrodynamic size distributions were single, narrow peaks (Figure 4B), suggesting no aggregation of SMB-2 brush molecules. The observed large and abrupt size transition of SMB-2 correlates well with the soluble-to-insoluble transition of PDEAEMA in water at pH values around its pK_a of ~ 7.4. We previously observed that when the pH was raised to near and above the pK_a, homografted PDEAEMA MBBs aggregated and precipitated out from the solution immediately even at very low concentrations (< 0.02 mg/g),[33] indicating the highly hydrophobic nature of PDEAEMA at higher pH values. For the present case of SMB-2, upon increasing pH from below to around the pK_a, the PDEAEMA side chains were deprotonated and became insoluble in water, driving the brushes to collapse into a compact structure that was manifested in a sharp and large size decrease; no aggregation and

precipitation of SMB-2 demonstrated that the collapsed brushes were effectively stabilized by the PEO side chains.

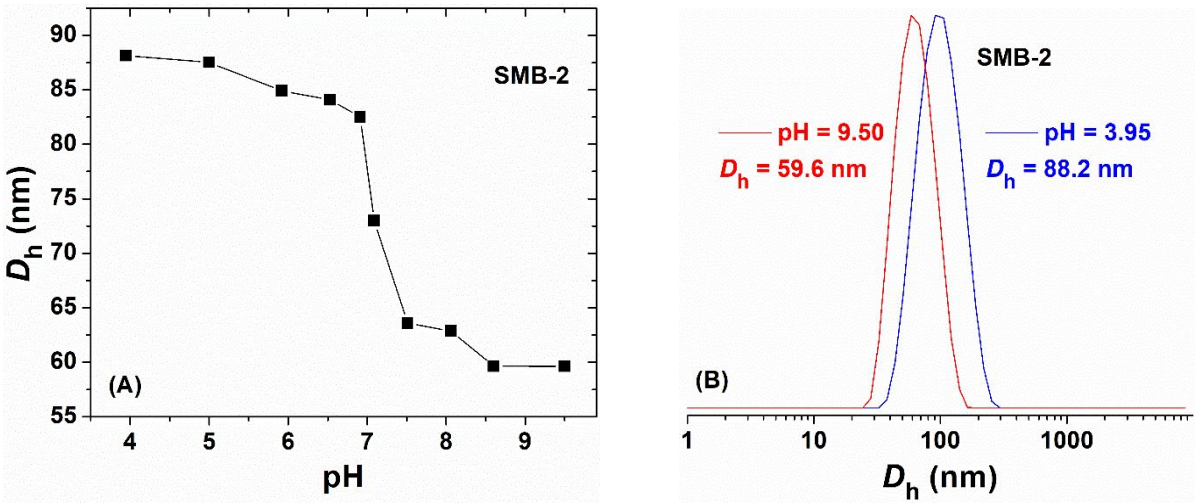

Figure 4. (A) Apparent hydrodynamic diameter (D_h) of SMB-2 at a concentration of 0.2 mg/g in a 10 mM phosphate buffer solution at 25 °C as a function of pH from a dynamic light scattering study. (B) Hydrodynamic size distributions of SMB-2 at pH = 3.95 and pH = 9.50.

The pH-induced large conformational change of SMB-2 was confirmed by AFM imaging. Figure 5A and S11 show the SMB-2 brush molecules spin cast on a glass disk from a 0.05 mg/g aqueous solution with a pH of 4.00. As expected, the brushes were in a starlike state; the average arm length from measurements of 75 arms was 99.8 ± 32.3 nm, slightly larger than that from THF (94.1 ± 30.3 nm, Figure 1B), and the typical height was ~ 2 nm (Figure 5B). Some of the brush molecules appeared to be missing an arm or have an unusually short arm, which could be caused by the mechanical shear force during the spin casting process. In contrast, the brushes from a 0.05 mg/g aqueous solution with a pH of 9.50 were in a collapsed globular state (Figures 5C and S12) with an average diameter of 53.4 ± 6.6 nm (100 measured) and a typical height of ~ 6 nm (Figure 5D). In some of the spherical nano-objects in Figure 5C, it is possible to see the contour of the raveled brush molecules, indicating that the observed species were indeed collapsed bottlebrushes. These AFM images demonstrated the pH-induced star-globule shape transition of SMB-2.

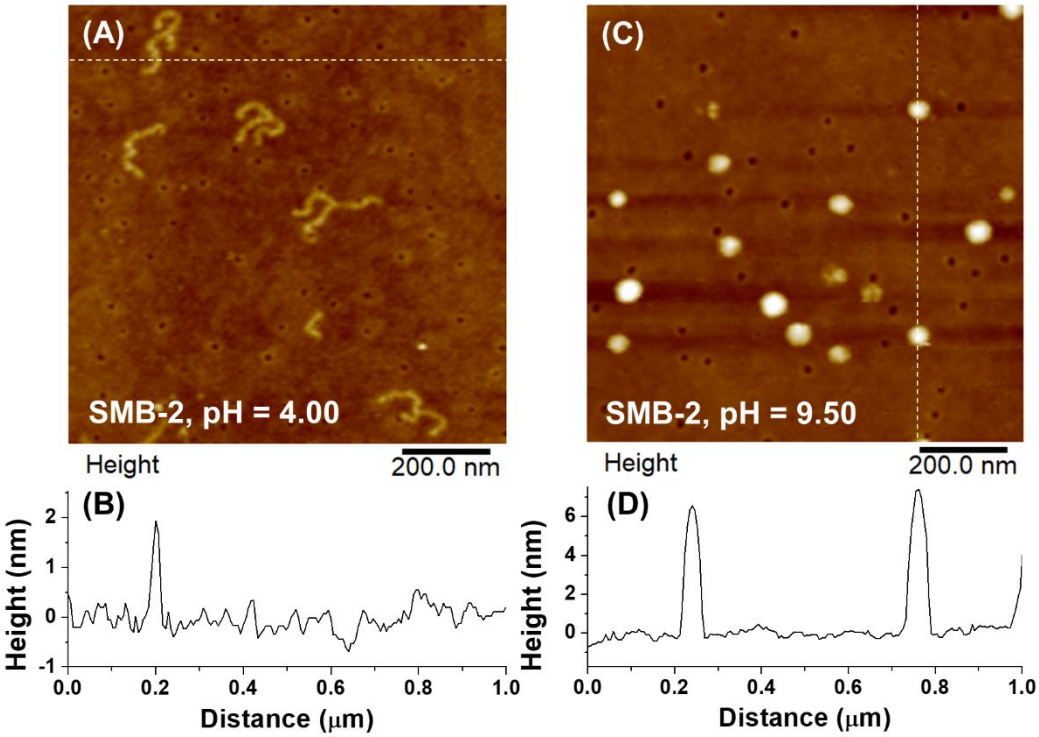

Figure 5. AFM height images of SMB-2 spin cast onto a glass disk from 0.05 mg/g aqueous solutions with (A) a pH of 4.00 and (B) a pH of 9.50. (B) and (D) Cross-sectional height profiles along the dashed lines in (A) and (C), respectively.

Chaotropic Anion-Induced Shape Changes of SMB-1 and -2 in Acidic Aqueous Solution.

Chaotropic ion pairing and chaotropic effect present new opportunities for design and attaining of self-assembled supramolecular polymer nanostructures in aqueous solution.[52,53] For example, Gao et al. reported the micellization of protonated tertiary amine-containing diblock copolymers in acidic aqueous solutions induced by CAs (ClO_4^-, SCN^-, etc.) when the alkyl substituents at the nitrogen atom were larger than the methyl group.[52] It is worth noting here that NH_4^+, $CH_3NH_3^+$, and $N^+(CH_3)_4$ are chaotropic cations, whereas $N^+(CH_2CH_3)_4$ is a borderline ion between water-structure breaking and making according to Macus.[43] Thus, the protonated monomer units of PDMAEMA and PDEAEMA in acidic aqueous solutions are very likely chaotropic cations. Here we show that CAs, such as ClO_4^-, can be employed to induce star-to-globule shape transitions of SMB-1 and -2 in acidic aqueous solutions and superchaotropic anions (e.g., $Fe(CN)_6^{3-}$ and $S_2O_8^{2-}$

) are much more efficient in triggering the brushes' conformational changes than moderate CAs (e.g., ClO_4^- and SCN^-).

Aqueous solutions of SMB-1 and -2 with a concentration of 0.1 mg/g in Milli-Q water were prepared and the pH was adjusted to 4.00 using 0.10 M HCl. A total of six salts were used in this study: $K_3[Fe(CN)_6]$, $K_2S_2O_8$, $NaClO_4$, NaSCN, NaBr, and NaCl. Cl^-, Br^-, SCN^-, and ClO_4^- are CAs with an effective loss of 1.01 – 1.27 hydrogen bonds in the solvation shell around the ion,[46] and their ability in water-structure breaking increases in the order of $Cl^- < Br^- < SCN^- < ClO_4^-$. In contrast, $Fe(CN)_6^{3-}$ and $S_2O_8^{2-}$ are superchaotropic anions with similar water-structure breaking abilities, causing a loss of about 2 surrounding hydrogen bonds.[46] K^+ is a weakly structure-breaking cation, while Na^+ is a borderline ion.[43] Thus, the effects observed in this study should predominantly come from the anions of the salts. For each salt, the concentration was gradually increased by adding a calculated amount of a stock solution for lower concentrations (≤ 10 mM) and a weighed amount of the salt in the solid form for concentrations beyond 10 mM.

Figure 6A shows the plots of D_h of SMB-1 as a function of the salt concentration for the six salts. For all the salts at a concentration of 0.01 mM, the apparent sizes were very similar (between 90 and 92 nm). However, the salts quickly differentiated themselves with increasing concentration. For superchaotropic ferricyanide anions, the D_h of the brushes decreased rapidly from 88.9 nm to 55.7 nm upon increasing the salt concentration from 0.05 mM to 0.1 mM, respectively, while maintaining a single, narrow size distribution (Figure 6B). Further increasing the $Fe(CN)_6^{3-}$ concentration to 0.5 mM, we began to see a small amount of large species by DLS in the 4000 – 5000 nm range (Figure 6B), likely due to the formation of some loose aggregates induced by the superchaotropic anion at this salt concentration. For $S_2O_8^{2-}$, the transition was somewhat broader than that with $Fe(CN)_6^{3-}$ and occurred at slightly higher concentrations; the size decreased from

88.4 to 61.7 nm with increasing [$S_2O_8^{2-}$] from 0.1 to 0.4 mM. This was followed by a much slower reduction of the size to 55.6 nm at 10.0 mM. For ClO_4^-, the sharp size transition occurred at much higher concentrations compared with the two superchaotropic anions, although the overall size change was similar, from 90.7 nm at 1.0 mM to 56.1 nm at 300 mM. At [ClO_4^-] = 600 mM, a small amount of large aggregates began to be observed (Figure S13). In contrast, the addition of SCN^-, Br^-, and Cl^- did not result in a sharp size decrease but a gradual and smaller change. The D_h decreased from 90.4 nm at 0.01 mM to 74.5 nm at 300 mM for SCN^- , from 91.0 nm at 0.01 mM to 77.8 nm at 500 mM for Br^-, and from 91.8 nm at 0.01 mM to 81.2 nm at 500 mM for Cl^-; the size reduction decreased in the order of $SCN^- > Br^- > Cl^-$. Clearly, stronger CAs cause larger and more abrupt changes in the size of SMB-1 at lower concentrations, while weaker CAs resulted in only small and gradual size changes even at rather high concentrations.

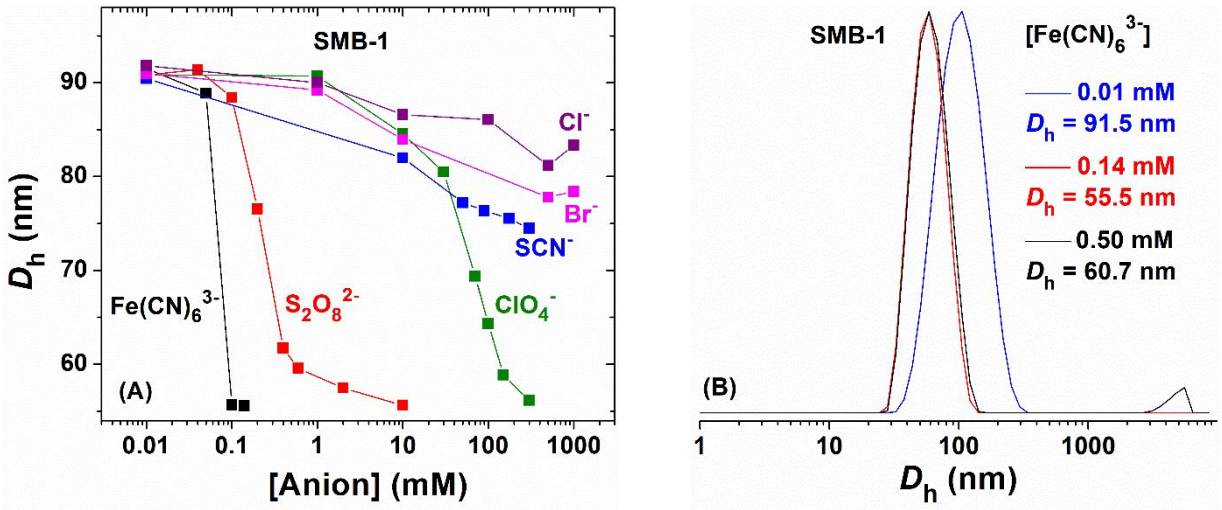

Figure 6. (A) Apparent hydrodynamic diameter (D_h) of 0.1 mg/g SMB-1 in water with a pH of 4.00 at 25 °C as a function of increasing concentration of a salt from DLS measurements for $K_3[Fe(CN)_6]$ (black), $K_2S_2O_8$ (red), $NaClO_4$ (green), NaSCN (blue), NaBr (pink), and NaCl (purple). All data points here are single size distributions. (B) Hydrodynamic size distributions of SMB-1 in water with a pH of 4.00 at ferricyanide concentrations of 0.01, 0.14, and 0.50 mM.

We then investigated the salt-responsive behavior of SMB-2 in water at a concentration of 0.1

mg/g with a pH of 4.00 by DLS. Figure 7A shows the change in D_h of SMB-2 with increasing salt concentration for the same six salts studied with SMB-1. For superchaotropic anions, $Fe(CN)_6^{3-}$ and $S_2O_8^{2-}$, the size transitions occurred over very similar salt concentration ranges to those observed for SMB-1. The D_h of SMB-2 decreased from 90.0 nm at the salt concentration of 0.04 mM to 57.0 nm at 0.18 mM for $Fe(CN)_6^{3-}$ and 89.0 nm at 0.04 mM to 62.2 nm at 1.0 mM for $S_2O_8^{2-}$, while maintaining single narrow size distributions (Figure 7B shows the size distributions for $Fe(CN)_6^{3-}$ at the concentrations of 0.01 and 0.50 mM). Interestingly, for ClO_4^-, the size transition of SMB-2 occurred in a lower concentration range, between 2.0 mM (D_h = 86.7 nm) and 50.0 mM (D_h = 60.1 nm), than SMB-1 (from D_h = 90.7 nm at 1.0 mM to 56.1 nm at 300 mM). For SCN^-, SMB-2 showed a gradual size change from 90.8 to 74.0 nm with increasing the salt concentration from 0.01 to 120 mM, respectively, followed by a steeper decrease to 63.0 nm at 500 mM with a single size distribution (Figure S14); unlike SMB-1, which showed only a gradual decrease in the D_h over the [SCN^-] range of 0.01 to 300 mM with the smallest size of 74.5 nm observed at 300 mM (Figures 6A and S13), the size transition of SMB-2 was larger and also sharper. On the other hand, Br^- and Cl^- exerted a rather small effect on the size of SMB-2, similar to that for SMB-1; both anions only reduced the D_h from ~ 91 nm at 0.01 mM to ~ 83 nm at 100 mM before leveling off. The effect of increasing the length of the two symmetric alkyl substituents at the nitrogen atom from methyl to ethyl was not apparent with superchaotropic $Fe(CN)_6^{3-}$ and $S_2O_8^{2-}$ anions and very weakly chaotropic Br^- and Cl^- anions, but became more evident with moderate CAs (ClO_4^- and SCN^-). As mentioned earlier, $(CH_3)_4N^+$ is a chaotropic cation, while $(C_2H_5)_4N^+$ is a borderline ion between chaotropic and kosmotropic cations according to Marcus.[43] Thus, by analogy, the protonated tertiary amine moieties of PDEAEMA, $-CH_2CH_2N^+H(C_2H_5)_2$, should be a weaker chaotropic cation than those of PDMAEMA, $-CH_2CH_2N^+H(CH_3)_2$, under the

same conditions. Accordingly, the ion pairing should be weaker for protonated PDEAEMA side chains; however, this is not consistent with our observations. The stronger effect of ClO_4^- on the size transition of SMB-2 than that of SMB-1, as indicated by the collapse of the brushes at lower concentrations, likely comes from the chaotropic effect[46] that CAs have a high propensity to associate with the more hydrophobic ethyl groups of PDEAEMA side chains in addition to ion pairing. The observation that SCN^- collapsed SMB-2 but not SMB-1 at a concentration of 300 mM can be primarily attributed to the chaotropic effect – the stronger association to the more hydrophobic groups of PDEAEMA side chains.

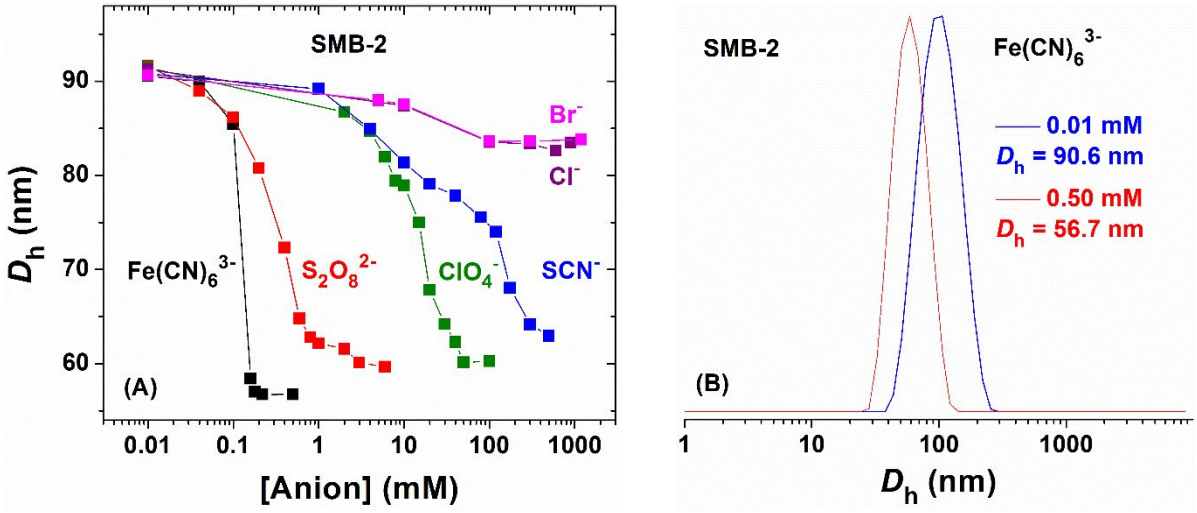

Figure 7. (A) Apparent hydrodynamic diameter (D_h) of 0.1 mg/g SMB-2 in water with a pH of 4.00 at 25 °C as a function of increasing concentration of a salt from DLS measurements for $K_3[Fe(CN)_6]$ (black), $K_2S_2O_8$ (red), $NaClO_4$ (green), NaSCN (blue), NaBr (pink), and NaCl (purple). All datapoints here are single size distributions. (B) Hydrodynamic size distributions of SMB-2 in water with a pH of 4.00 at $[Fe(CN)_6^{3-}]$ of 0.01 and 0.50 mM.

The observed effects of different CAs on the hydrodynamic sizes of SMB-1 and -2 follow the chaotropicity scale based on the ion hydration parameters proposed by Marcus: $Cl^- < Br^- < SCN^- < ClO_4^- << S_2O_8^{2-} \sim Fe(CN)_6^{3-}$.[46] The large and sharp size reductions induced by stronger CAs (ClO_4^-, $S_2O_8^{2-}$, and $Fe(CN)_6^{3-}$ for both SMB-1 and -2 and SCN^- for SMB-2) are believed to result from the enthalpically favorable formation and clustering of tight ion pairs with ammonium cations

(-$OCH_2CH_2N^+H(CH_3)_2$ and -$OCH_2CH_2N^+H(C_2H_5)_2$)) as well as the aforementioned chaotropic effect for SMB-2. These effects severely decreased the solubility of the tertiary amine-containing side chains and forced the brushes to collapse into more compact structures, stabilized by the soluble PEO side chains, in order to minimize the contact with water. Note that superchaotropic $Fe(CN)_6^{3-}$ and $S_2O_8^{2-}$ anions have very similar water-structure breaking abilities with a loss of 2.01 surrounding hydrogen bonds for $Fe(CN)_6^{3-}$ and 2.04 hydrogen bonds for $S_2O_8^{2-}$.[43,46] The observed stronger effect of $Fe(CN)_6^{3-}$ for both SMB-1 and -2 than $S_2O_8^{2-}$, as evidenced by the lower concentrations to collapse the brushes, might be related to the trivalency of $Fe(CN)_6^{3-}$, which could interact simultaneously with three monovalent cations. It should be noted here that Müller et al. observed the formation of helical and spherical nanostructures of homografted poly(methacryloylethyl trimethylamine iodide) MBBs in very dilute aqueous solutions after the addition of di- and trivalent anions, which was attributed to the multivalency of the ions.[28]

To confirm our hypothesis of the solubility changes of protonated PDMAEMA side chains in SMB-1 and PDEAEMA side chains in SMB-2 with the addition of strong CAs, we conducted ^1H NMR spectroscopy analysis using 4.0 mg/g solutions of SMB-1 and SMB-2 in D_2O at a pH of 4.00 with the gradual addition of $K_3[Fe(CN)_6]$ (Figure 8). For SMB-1, the characteristic peaks of the PDMAEMA side chains were clearly visible at 4.58 – 4.16 ppm [-OC$H_2$$CH_2N^+H(CH_3)_2$], 3.67 – 3.41 ppm [-$OCH_2CH_2N^+H(CH_3)_2$], and 3.20 – 2.83 ppm [-$OCH_2CH_2N^+H(CH_3)_2$] before the addition of $K_3[Fe(CN)_6]$. Increasing $[Fe(CN)_6^{3-}]$ to 0.1 mM resulted in the broadening of these peaks and the almost disappearance of the peaks at ~ 1 and ~ 2 ppm (corresponding to -C(CH_3)- and -CH_2- of the PDMAEMA backbone, respectively). At 1.0 and 2.0 mM of $Fe(CN)_6^{3-}$, the peaks at 4.58 – 4.16, 3.67 – 3.41, and 3.20 – 2.83 ppm were severely diminished and largely invisible. Note that in the DLS measurements, the polymer concentration was 0.1 mg/mL, corresponding to

a molar concentration of ammonium cations of 0.32 mM, and the full collapse was observed at 0.1 mM of $Fe(CN)_6^{3-}$. Thus, the molar ratio of $Fe(CN)_6^{3-}$ to ammonium is ~ 0.3 : 1, which is on the same order of the molar ratio observed from the ^1H NMR spectroscopy study (~ 0.1 : 1) at the $Fe(CN)_6^{3-}$ concentration of 1.0 mM for 4.0 mg/g SMB-1. At all concentrations studied, the characteristic peak for the PEO side chains at 3.72 ppm (-OCH_2CH_2-) remained sharp and decreased only slightly in intensity relative to the residual solvent proton signal.

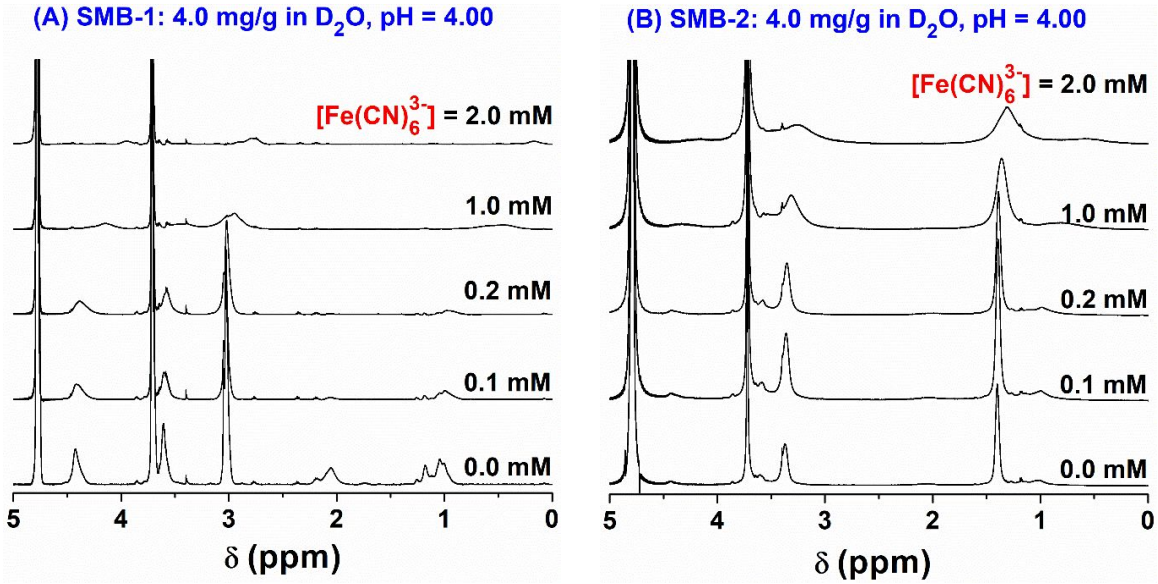

Figure 8. ^1H NMR spectra of 4.0 mg/g SMB-1 (A) and SMB-2 in D_2O with a pH of 4.00 in the presence of $Fe(CN)_6^{3-}$ with various concentrations. All spectra are normalized to the residual HDO peak at 4.79 ppm.

Similarly, for SMB-2, the characteristic peaks of the PEO side chains at 3.72 ppm and the protonated PDEAEMA side chains at 3.48 – 3.21 ppm [-$OCH_2CH_2N^+H(CH_2CH_3)_2$], and 1.53 – 1.30 ppm [-$OCH_2CH_2N^+H(CH_2CH_3)_2$] were visible and relatively sharp before the addition of $K_3[Fe(CN)_6]$ (Figure 8B). With increasing $[Fe(CN)_6^{3-}]$, the PEO peak remained sharp, whereas the PDEAEMA peaks broadened significantly at the $Fe(CN)_6^{3-}$ concentrations of 1.0 and 2.0 mM, which are similar to the observations for SMB-1. However, the PDEAEMA peaks remained visible,

in contrast to SMB-1 where the peaks largely disappeared, suggesting that the ion pairs of $Fe(CN)_6^{3-}$ and the protonated repeat units of PDMAEMA were likely tighter. For comparison, we also gradually added NaCl into the solutions of SMB-1 and -2 in D_2O at a pH of 4.00 and collected the ^1H NMR spectra (Figure S15). All of the characteristic peaks of the protonated tertiary amine groups remained visible and relatively sharp even at the NaCl concentration of 100 mM and no any peaks became broadened or disappeared, consistent with the observations from the DLS studies that the size changes were small.

AFM was then used to visualize the SMB-1 and -2 brush molecules from their aqueous solutions with a pH of 4.00 in the presence of $K_3[Fe(CN)_6]$. Figures 9 and S16 show the AFM height images of the SMB-1 molecules drop cast on a glass disk from a 0.05 mg/g aqueous solution at pH = 4.00 in the presence of 0.14 mM $K_3[Fe(CN)_6]$, under which from the DLS study SMB-1 fully collapsed (Figure 6A). Indeed, globular nano-objects with an average diameter of 49.7 ± 8.7 nm from the measurements of 100 brush molecules were observed, and the typical height of the globular brush molecules was ~ 11 nm (Figure 9C). In Figure 9A, a few unraveled brushes in the starlike state could be seen, likely due to the shear force from blowing of the brush solution off the disk with a stream of nitrogen in the sample preparation. AFM imaging also revealed the collapsed globular brush molecules for SMB-2 prepared under the same conditions as for SMB-1 (Figures 10 and S17). The average diameter of the collapsed globular nano-objects from the measurements of 100 molecules was 57.3 ± 7.2 nm and the typical height was also ~ 11 nm. For comparison, we also conducted AFM imaging of SMB-1 and -2 drop cast on glass disks from 0.05 mg/g aqueous solutions with a pH of 4.00 in the presence of 100 mM NaCl; as expected from the DLS and ^1H NMR spectroscopy studies, starlike bottlebrush molecules were seen for both SMB-1 and -2 (Figures S18 and S19).

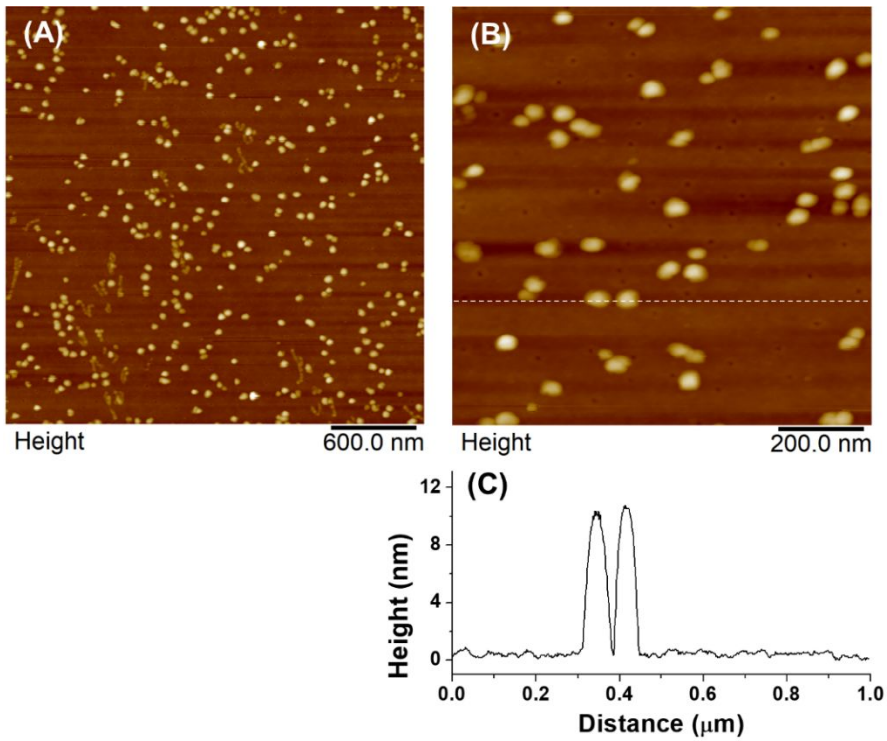

Figure 9. (A) and (B) AFM height images of SMB-1 drop cast onto a glass disk from a 0.05 mg/g aqueous solution at pH = 4.00 with 0.14 mM $K_3[Fe(CN)_6]$. (C) Cross-sectional height profile along the dashed line in (B).

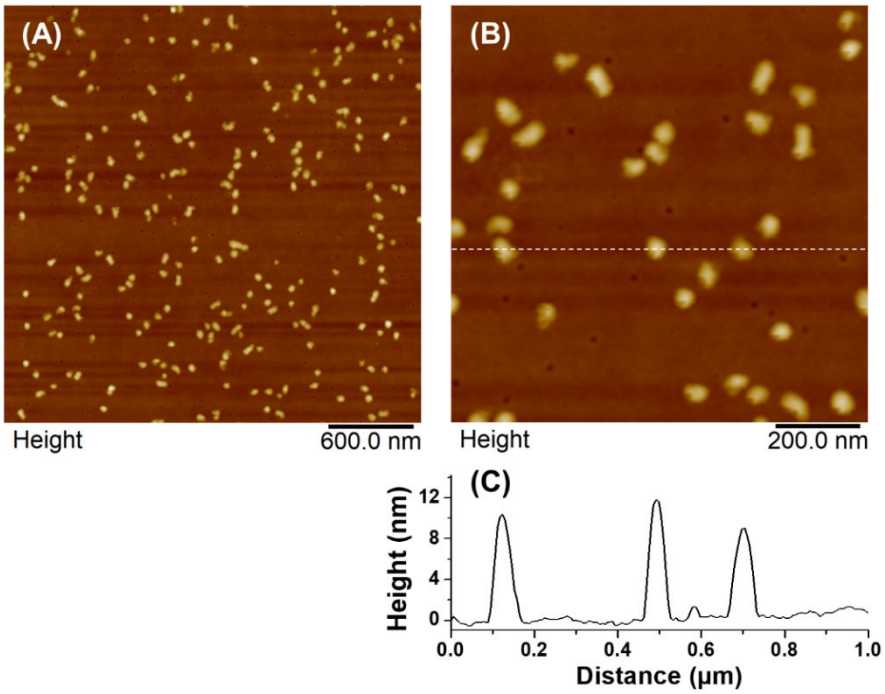

Figure 10. (A) and (B) AFM height images of SMB-2 drop cast onto a glass disk from a 0.05 mg/g aqueous solution at pH = 4.00 with 0.14 mM $K_3[Fe(CN)_6]$. (C) Cross-sectional height profile along the dashed line in (B).

Conclusions

In conclusion, we synthesized binary heterografted three-arm star MBBs, SMB-1 composed of PEO and PDMAEMA side chains and SMB-2 with PEO and PDEAEMA side chains, via a click grafting to method and demonstrated that these brushes underwent stimuli-induced conformational changes in aqueous solutions. While SMB-1 exhibited only a small decrease in the D_h and no shape transition with increasing pH from below to above the pK_a of PDMAEMA, SMB-2 showed a large and abrupt size transition at pH around the pK_a of PDEAEMA, and the pH-induced star-to-globule shape transition was revealed by AFM with starlike brushes observed at pH = 4.00 and globular nano-objects at pH = 9.50. In addition, both SMB-1 and -2 underwent star-to-globule shape transitions in acidic aqueous solutions in response to the addition of sufficiently strong CAs. Superchaotropic $Fe(CN)_6^{3-}$ and $S_2O_8^{2-}$ anions were more efficient in inducing the shape transitions of both brush polymers. On the other hand, weak chaotropic Cl^- and Br^- anions had rather small effects on the hydrodynamic size of either brushes. The CA-triggered shape changing of MBBs was attributed to the formation of tight ion-pairs with ammonium cations, leading to the insolubility of tertiary amine-containing side chains. SMB-2 displayed a greater sensitivity to moderate CAs (ClO_4^- and SCN^-) than SMB-1, likely due to the chaotropic effect in addition to ion pairing. We believe that the results reported here enrich the concepts of shape-changing MBBs and chaotropic effect-driven supramolecular assembly and might have implications in potential applications such as encapsulation and release of charged substances.

Conflicts of interest: There are no conflicts to declare.

Electronic Supplementary Information Available. Experimental section and calculation of grafting densities of SMB-1 and -2; characterization data for side chain polymers, crude and

purified star MBBs; additional AFM images of star brushes; hydrodynamic size distributions of SMB-1 and -2 in water at pH = 4.00 with various salts of different concentrations; ^{1}H NMR spectra of SMB-1 and -2 in D_2O at pH = 4.0 in the presence of NaCl; AFM images of SMB-1 and -2 from aqueous solutions with a pH of 4.00 in the presence of 100 mM NaCl. The Electronic Supplementary Information is available free of charge on the website at DOI: xxxxxxxxxxxxx.

Acknowledgements: This work was supported by NSF through DMR-1607076 and -2004564.

References:

1. J. Y. Yuan, A. H. E.Muller, K. Matyjaszewski, S. S. Sheiko, *Polymer Science: A Comprehensive Reference, 10 Volume Set*, Elsevier: 2012; Vol. 6, pp 199-264.
2. M. Zhang, A. H. E. Müller, *J. Polym. Sci. Part A: Polym. Chem.*, 2005**, 43**, 3461-3481.
3. S. S. Sheiko, B. S. Sumerlin, K. Matyjaszewski, *Prog. Polym. Sci.*, 2008**, 33**, 759-785.
4. H.-i. Lee, J. Pietrasik, S. S. Sheiko, K. Matyjaszewski, *Prog. Polym. Sci.*, 2010**, 35**, 24-44.
5. G. Xie, M. R. Martinez, M. Olszewski, S. S. Sheiko, K. Matyjaszewski, *Biomacromolecules*, 2019**, 20**, 27-54.
6. S. S. Sheiko, F. C. Sun, A. Randal, D. Shirvaniants, H.-i. Lee, K. Matyjaszewski, *Nature* 2006, **440**, 191–194.
7. W. F. Daniel, J. Burdynska, M. Vatankhah-Varnoosfaderani, K. Matyjaszewski, J. Paturej, M. Rubinstein, A. V. Dobrynin, S. S. Sheiko, *Nat. Mater.*, 2016, **15**, 183−189.
8. X. Banquy, J. Burdyńska, D. W. Lee, K. Matyjaszewski, J. Israelachvili, *J. Am. Chem. Soc.*, 2014**, 136**, 6199-6202.
9. H. Qi, X. T. Liu, D. M. Henn, S. Mei, M. C. Staub, B. Zhao, C. Y. Li, *Nat. Commun.*, 2020, **11**, 2152.
10. S. S. Sheiko, S. A. Prokhorova, K. L. Beers, K. Matyjaszewski, I. I. Potemkin, A. R. Khokhlov, M. Möller, *Macromolecules*, 2001, **34**, 8354−8360.
11. J. R. Boyce, D. Shirvanyants, S. S. Sheiko, D. A. Ivanov, S. H. Qin, H. G. Börner, K. Matyjaszewski, *Langmuir*, 2004, **20**, 6005–6011.
12. M. O. Gallyamov, B. Tartsch, A. R. Khokhlov, S. S. Sheiko, H. G. Börner, K. Matyjaszewski, M. Möller, *Chem. Eur. J.*, 2004, **10**, 4599–4605.
13. M. O. Gallyamov, B. Tartsch, A. R. Khoklov, S. S. Sheiko, H. G. Börner, K. Matyjaszewski, M. Möller, *Macromol. Rapid Comm.*, 2004, **25**, 1703-1707.
14. C. Li, N. Gunari, K. Fischer, A. Janshoff, M. Schmidt, *Angew. Chem., Int. Ed.*, 2004, **43**, 1101−1104.
15. H.-i. Lee, J. Pietrasik, K. Matyjaszewski, *Macromolecules*, 2006, **39**, 3914−3920.
16. S.-i. Yamamoto, J. Pietrasik, K. Matyjaszewski, *Macromolecules*, 2007, **40**, 9348−9353.
17. J. Pietrasik, B. S. Sumerlin, R. Y. Lee, K. Matyjaszewski, *Macromol. Chem. Phys.*, 2007, **208**, 30−36.
18. H.-i. Lee, J. R. Boyce, A. Nese, S. S. Sheiko, K. Matyjaszewski, *Polymer*, 2008, **49**, 5490−5496.
19. Y. Y. Xu, S. Bolisetty, M. Drechsler, B. Fang, J. Yuan, M. Ballauff, A. X. E. Müller, *Polymer*, 2008, **49**, 3957−3964.

20. W. Liu, Y. Liu, G. Zeng, R. Liu, Y. Huang, *Polymer*, 2012, **53**, 1005–1014.
21. X. Li, H. ShamsiJazeyi, S. L. Pesek, A. Agrawal, B. Hammouda, R. Verduzco, *Soft Matter*, 2014, **10**, 2008−2015.
22. E. Kutnyanszky, M. A. Hempenius, G. J. Vancso, *Polym. Chem.*, 2014, **5**, 771−783.
23. W. X. Dai, X. M. Zhu, J. Zhang, Y. L. Zhao, *Chem. Commun.*, 2019, **55**, 5709–5712.
24. X. M. Zhu, J. Zhang, C. Miao, S. Y. Li, Y. L. Zhao, *Polym. Chem.* 2020, **11**, 3003-3017.
25. Y. Y. Yan, C Gao, J. J. Li, T. Zhang, G. Yang, Z. K. Wang, Z. Hua, *Biomacromolecules*, 2020, **21**, 613-620.
26. Y. Y. Xu, S. Bolisetty, M. Ballauff, A. X. E. Müller, *J. Am. Chem. Soc.*, 2009, **131**, 1640−1641.
27. Y. Y. Xu, O. V. Borisov, M. Ballauff, A. X. E. Müller, *Langmuir* 2010, **26**, 6919–6926.
28. Y. Y. Xu, S. Bolisetty, M. Drechsler, B. Fang, J. Yuan, L. Harnau, M. Ballauff, A. H. E. Müller, *Soft Matter*, 2009, **5**, 379−384.
29. N. Gunari, Y. Cong, B. Zhang, K. Fischer, A. Janshoff, M. Schmidt, *Macromol. Rapid Commun.*, 2008, **29**, 821−825.
30. Y. Cong, N. Gunari, B. Zhang, A. Janshoff, M. Schmidt, *Langmuir*, 2009, **25**, 6392–6397.
31. D. M. Henn, W. X. Fu, S. Mei, C. Y. Li, B. Zhao, *Macromolecules*, 2017, **50**, 1645-1656.
32. D. M. Henn, C. M. Lau, C. Y. Li, B. Zhao, *Polym. Chem.*, 2017, **8**, 2702-2712.
33. E. W. Kent, D. M. Henn, B. Zhao, *Polym. Chem.*, 2018, **9**, 5133-5144.
34. E. W. Kent, B. Zhao, *Macromolecules*, 2019, **52**, 6714-6724.
35. D. M. Henn, J. A. Holmes, E. W. Kent, B. Zhao, *J. Phys. Chem. B*, 2018, **122**, 7015-7025.
36. D. Han, X. Tong, Y. Zhao, *Macromolecules*, 2011, **44**, 5531−5536.
37. H. Tang, Y. Li, S. H. Lahasky, S. S. Sheiko, D. H. Zhang, *Macromolecules*, 2011, **44**, 1491−1499.
38. P. Zhao, Y. Yan, X. Feng, L. Liu, C. Wang, Y. Chen, *Polymer*, 2012, **53**, 1992-2000.
39. Y. Shi, X. Cao, H. F. Gao, *Nanoscale*, 2016, **8**, 4864-4881.
40. H. Luo, M. Szymusiak, E. A. Garcia, L. L. Lock, H. Cui, Y. Liu, M. Herrera-Alonso, *Macromolecules*, 2017, **50**, 2201−2206.
41. Y. M. Mo, G. J. Liu, Y. Y. Tu, S. D. Lin, J. Song, J. W. Hu, F. Liu, *J. Polym. Sci., Part A: Polym. Chem.*, 2017, **55**, 1021-1030.
42. E. W. Kent, E. M. Lewoczko, B. Zhao, *Langmuir* 2020, **36**, 13320-13330.
43. Y. Marcus, *Chem. Rev.*, 2009, **109**, 1346–1370.
44. K. D. Collins, *Biophys. J.*, 1997, **72**, 65-76.
45. Y. Marcus, G. Hefter, *Chem. Rev.*, 2006, **106**, 4585-4621.
46. K. I. Assaf, W. M. Nau, *Angew. Chem. Int. Ed.* **2018**, *57*, 13968–13981.
47. L. D. Liu, R. Kou, G. M. Liu, *Soft Matter*, 2017, **13**, 68-80.
48. H. Y. Yuan, G. M. Liu, *Soft Matter*, 2020, **16**, 4087-4104.
49. K. J. Zhou, Y. G. Wang, X. N. Huang, K. Luby-Phelps, B. D. Sumer, J. M. Gao, *Angew. Chem. Int. Ed.*, 2011, **50**, 6109−6114.
50. D. M. Henn, R. A. E. Wright, J. W. Woodcock, B. Hu, B. Zhao, *Langmuir*, 2014, **30**, 2541–2550.
51. R. A. E. Wright, D. M. Henn, B. Zhao, *J. Phys. Chem. B*, 2016, **120**, 8036-8045.
52. Y. Li, Y. G. Wang, G. Huang, X. P. Ma, K. J. Zhou, J. M. Gao, *Angew. Chem. Int. Ed.* **2014**, *53*, 8074 –8078.
53. L.-H. Wang, Z.-D. Zhang, C.-Y. Hong, X.-H. He, W. You, Y.-Z. You, *Adv. Mater.*, 2015, **27**, 3202–3207.

For Table of Contents Graphic Use Only

Title: pH- and Chaotropic Anion-Induced Conformational Changes of Tertiary Amine-Containing Binary Heterografted Star Molecular Bottlebrushes in Aqueous Solution

Authors: *Ethan W. Kent, Evan M. Lewoczko, and Bin Zhao*

Table of Contents Entry Graphic:

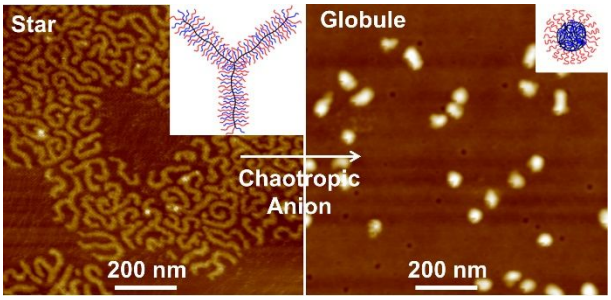

Table of Contents Entry Graphical Abstract: Three-arm star-shaped, tertiary-amine-containing bottlebrushes exhibit star-globule shape transitions in response to pH changes and addition of sufficiently strong chaotropic anions.